

SPITZER/MIPS INFRARED IMAGING OF M31: FURTHER EVIDENCE FOR A SPIRAL/RING COMPOSITE STRUCTURE

K. D. GORDON¹, J. BAILIN², C. W. ENGELBRACHT¹, G. H. RIEKE¹, K. A. MISSELT¹, W. B. LATTER³, E. T. YOUNG¹,
 M. L. N. ASHBY⁴, P. BARMBY⁴, B. K. GIBSON^{2,5}, D. C. HINES⁶, J. HINZ¹, O. KRAUSE¹, D. A. LEVINE⁷, F. R. MARLEAU⁷,
 A. NORIEGA-CRESPO⁷, S. STOLOGY⁷, D. A. THILKER⁸, AND M. W. WERNER⁹

ApJ Letters, in press

ABSTRACT

New images of M31 at 24, 70, and 160 μm taken with the Multiband Imaging Photometer for Spitzer (MIPS) reveal the morphology of the dust in this galaxy. This morphology is well represented by a composite of two logarithmic spiral arms and a circular ring (radius ~ 10 kpc) of star formation offset from the nucleus. The two spiral arms appear to start at the ends of a bar in the nuclear region and extend beyond the star forming ring. As has been found in previous work, the spiral arms are not continuous but composed of spiral segments. The star forming ring is very circular except for a region near M32 where it splits. The lack of well defined spiral arms and the prominence of the nearly circular ring suggests that M31 has been distorted by interactions with its satellite galaxies. Using new dynamical simulations of M31 interacting with M32 and NGC 205 we find that, qualitatively, such interactions can produce an offset, split ring like that seen in the MIPS images.

Subject headings: galaxies: individual (M31, M32, NGC 205) — galaxies: spiral — galaxies: ISM

1. INTRODUCTION

M31 is the nearest ($d \sim 780$ kpc, Stanek & Garnavich 1998; Rich et al. 2005) external spiral galaxy (Sb, Hubble 1929) making it one of the premier laboratories for understanding spiral galaxies like our own. Tracing the spiral structure in M31 is an obvious first step, which has been done with varying degrees of success for many years. However, the high inclination ($74\text{--}78^\circ$) of M31 makes it difficult to determine its large-scale structure. In particular, there is no clear consensus regarding the organization of spiral structure in this important galaxy. The earliest quantitative studies focused on optical tracers such as HII regions (Arp 1964; Baade & Arp 1964), OB associations (Hodge 1979; van den Bergh 1991), and dark nebulae (Hodge 1980). These studies generally found structures consistent with a two-armed spiral (for the case for a one-armed spiral see Simien et al. 1978), but invoked disturbances such as varying inclinations and warps to account for the deviations from simple logarithmic spirals. More recently, HI (Guibert 1974; Braun 1991) and CO (Loinard et al. 1999; Nieten et al. 2005) have been

used. The velocity information available for these gas tracers can be used to disentangle the pileup of information due to M31's high inclination. These studies have found strong evidence for a two-armed spiral structure, but still suffer from the difficulty in connecting spiral arm segments into a coherent pattern.

The difficulty in finding coherent spiral structure in M31 is plausibly related to the interactions of M31 with its two nearest satellites, M32 and NGC 205. Disturbances in M31 are revealed by tidal features far outside M31's disk visible in deep, wide-field optical imaging (Ibata et al. 2001, 2005; Ferguson et al. 2002; Lewis et al. 2004). M32 is understood to be the perturber of the spiral arms (Byrd 1978, 1983) while NGC 205 has been modeled as the cause of the warp seen in the optical and HI disk of M31 (Sato & Sawa 1986). Quantifying the effects of M31's satellite galaxies is complicated by the lack of measured proper motions and uncertainties in relative distances (e.g. McConnachie et al. 2005).

Another difficulty in quantifying M31's spiral structure has been the lack of appropriate tracers in the innermost regions of the galaxy. Optical tracers are overwhelmed by the bright stellar bulge, while HI and CO, which would be easily seen through the bulge, are largely absent (Brinks & Shane 1984; Melchior et al. 2000) as the interstellar medium (ISM) in the central region is composed mainly of ionized gas (Devereux et al. 1994). The far-infrared (far-IR) emission can circumvent these difficulties as it traces the dust in M31, which penetrates the stellar bulge and should trace all phases of the ISM.

The first far-IR images of M31 were obtained with the Infrared Astronomical Satellite (IRAS) at 12, 25, 60, and 100 μm . The most prominent feature in these images is the bright, ~ 10 kpc radius, ring of star formation (Habing et al. 1984; Rice 1993) seen previously in H α images (Arp 1964; Devereux et al. 1994). The Infrared Space Observatory (ISO) imaged M31 at 175 μm finding both the bright ring and a fainter ring at larger radii (Haas et al. 1998). The Midcourse Space Experiment

¹ Steward Observatory, University of Arizona, Tucson, AZ 85721, (kgordon,cengelbracht,grieke,kmisselt,eyoung,jhinz,okrause)@as.arizona.edu

² Centre for Astrophysics and Supercomputing, Swinburne University of Technology, P.O. Box 218, Hawthorn, VIC 3122, Australia, jbailin@astro.swin.edu.au

³ NASA Herschel Science Center, 100-22, Caltech, Pasadena, CA 91125, latter@ipac.caltech.edu

⁴ Harvard-Smithsonian Center for Astrophysics, Cambridge, MA 02138, (mashby,pbarmby)@cfa.harvard.edu

⁵ Centre for Astrophysics, University of Central Lancashire, Preston, PR1 2HE, UK, bkgibson@uclan.ac.uk

⁶ Space Science Institute, 4750 Walnut Street, Boulder, CO 80301, dean.hines@colorado.edu

⁷ Spitzer Science Center, 220-6, Caltech, Pasadena, CA 91125, (deblev,marleau,alberto,stology)@ipac.caltech.edu

⁸ Center for Astrophysical Sciences, Johns Hopkins Univ., Baltimore, MD 21218, dthilker@pha.jhu.edu

⁹ Jet Propulsion Laboratory, MC 264-767, Pasadena, CA 91109, mww@ipac.caltech.edu

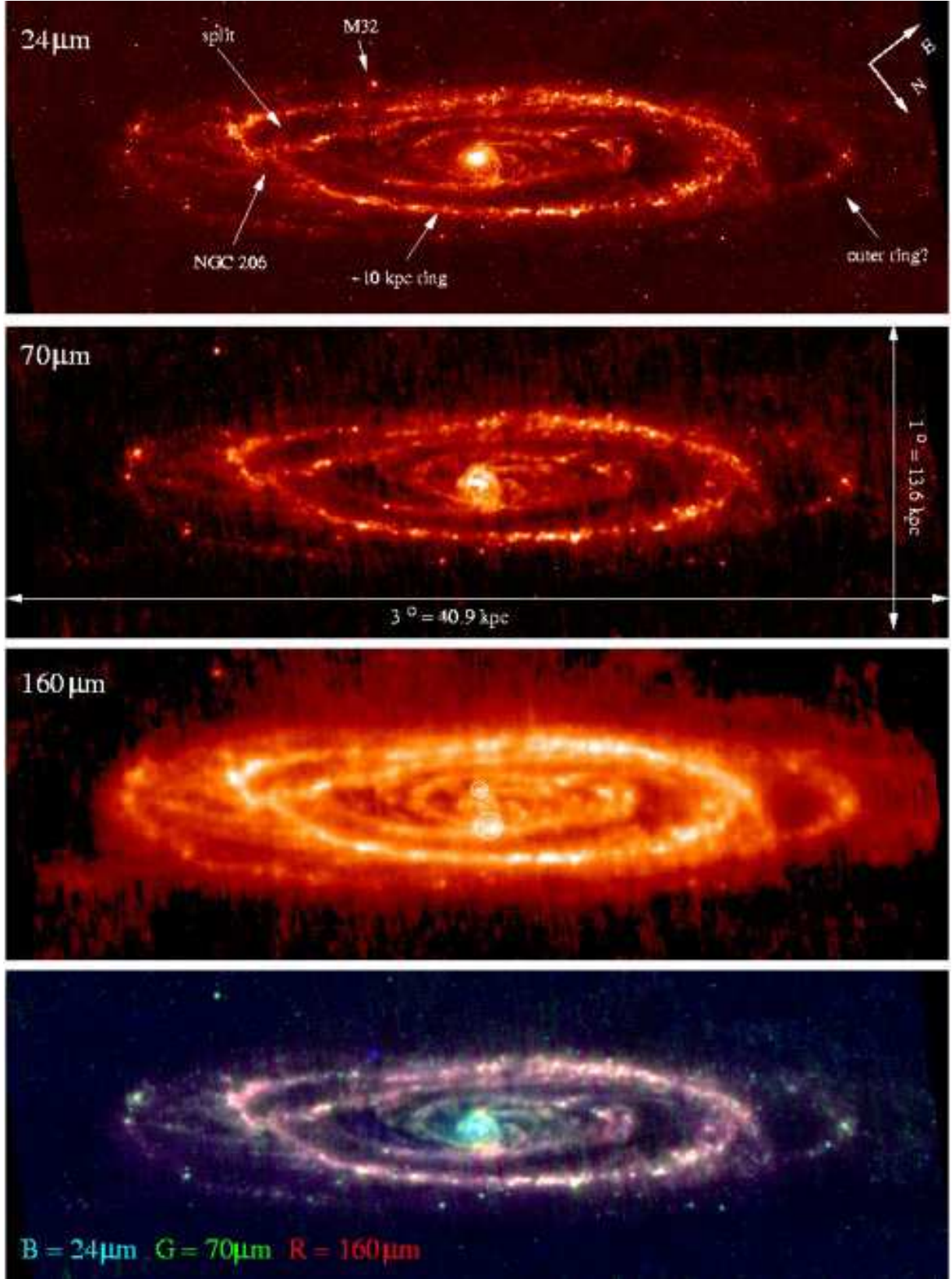


FIG. 1.— The M31 MIPS images are shown. The images are scaled using a quadratic root ($x^{0.25}$) between $-0.1 - 3$ MJy/sr ($24 \mu\text{m}$), $0.1 - 35$ MJy/sr ($70 \mu\text{m}$), and $0 - 90$ MJy/sr ($160 \mu\text{m}$). The bottom image gives the 3 color composite of the MIPS images (with scaling adjusted to emphasize the differences between bands); the color gives an indication of the dust temperature. The images are oriented with the nominal position angle of M31 (38°) horizontal and are cropped to a common size. The nearly-vertical streaks present in the 70 and $160 \mu\text{m}$ images are residual Ga:Ge detector instrumental signatures. M32 is clearly detected at $24 \mu\text{m}$, but not in the other two MIPS bands. NGC 205 is detected in all three MIPS bands, but is located NW of M31 beyond the boundary of the cropped images. The two spots near the nucleus marked on the $160 \mu\text{m}$ image are discussed in the text.

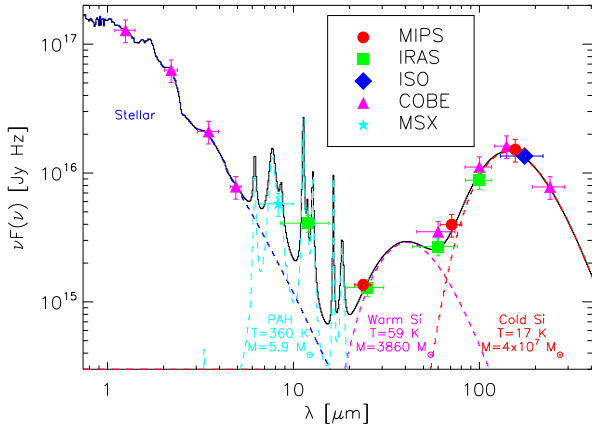


FIG. 2.— The MIPS global fluxes of M31 are plotted along with previous measurements from IRAS (Rice et al. 1988), COBE (Odenwald et al. 1998), ISO (Haas et al. 1998), and MSX (Kraemer et al. 2002). A simple stellar population plus dust grain model (Marleau et al., in prep.) has been fit to the data giving a total IR luminosity of 1.7×10^{43} ergs s^{-1} which corresponds to a star formation rate of $0.75 M_{\odot} \text{ yr}^{-1}$ using the calibration of Kennicutt (1998).

(MSX) provided an image of M31 at $8.3 \mu\text{m}$ revealing possible spiral structure inside the ~ 10 kpc ring. The resolutions of the IRAS ($\sim 1'$) and ISO ($1/3$) images reveal the overall morphology, but are not high enough to reveal the structure of the spiral arms.

We present new infrared images of M31 taken with the Multiband Imaging Photometer for Spitzer (MIPS, Rieke et al. 2004) instrument on the Spitzer Space Telescope (Spitzer, Werner et al. 2004). The MIPS spatial resolution at the distance of M31 is $6''/23$ pc, $18''/68$ pc, and $40''/151$ pc at 24 , 70 , and $160 \mu\text{m}$, respectively. This paper concentrates on the newly-revealed details of M31's infrared morphology as shown in the MIPS images

2. DATA

The MIPS images of M31 were taken on 25 Aug 2004. A region approximately $1^{\circ} \times 3^{\circ}$ oriented along the major axis of M31 was covered with 7 scan maps. Each map consisted of medium rate scan legs and cross scan offsets of $148''$ with lengths varying between $0^{\circ}75$ and $1^{\circ}25$ to efficiently map M31 and its satellite galaxy NGC 205. The MIPS DAT v2.90 (Gordon et al. 2005) was used to process and mosaic the individual images. At $24 \mu\text{m}$ extra steps were carried out to improve the images including readout offset correction, array averaged background subtraction (using a low order polynomial fit to each leg, with the region including M31 excluded from this fit), and exclusion of the 1st five images in each scan leg due to boost frame transients. At 70 and $160 \mu\text{m}$, the extra processing step was a pixel dependent background subtraction for each map (technique same as $24 \mu\text{m}$). The background subtraction does not remove real M31 emission as the scan legs are nearly parallel to the minor axis with the background regions being far from M31's disk. The final mosaics have exposure times of ~ 100 , ~ 40 , and ~ 9 seconds/pixel for 24 , 70 , and $160 \mu\text{m}$, respectively, and are shown in Figure 1.

The IR spectral energy distribution of M31 is shown in Fig. 2. The global MIPS fluxes measured in a $2^{\circ}75 \times 0^{\circ}75$

rectangular aperture (the background was subtracted in the data reduction) are 107 ± 10.7 , 940 ± 188 , and 7900 ± 1580 Jy for 24 , 70 , and $160 \mu\text{m}$, respectively. The uncertainties are dominated by the systematic uncertainties in the MIPS calibration (Rieke et al. 2004). There is excellent agreement between the MIPS and previous IR measurements.

3. MORPHOLOGY

The MIPS images in Fig. 1 are dominated by the ~ 10 kpc ring. The deprojected ISO image showed that the ring is fairly circular, but with an obvious splitting near the position of M32 (Haas et al. 1998). This splitting is now seen to extend over $\sim 1/4$ of the ring. The outer ring seen with ISO is seen in the MIPS images, but appears to be relatively incomplete. Overall, the morphology of the disk of M31 in the infrared appears more disturbed on the left-hand (southwest) than right-hand (northeast) side of the galaxy.

The MIPS images show emission extending beyond their edges along the major axis, implying that the infrared extent of M31 is larger than $3^{\circ}/40.9$ kpc. A comparison of the MIPS $160 \mu\text{m}$ image with the latest HI image (Braun et al., in prep.) reveals dust emission where there is HI emission. The gas and dust seem well mixed even in the outer regions of M31.

The infrared emission in the nuclear region has a component with hotter dust than the rest of M31 (but also a cold component due to the emission seen in the $160 \mu\text{m}$ image). This is consistent with the nuclear region gas being dominated by ionized gas as seen in H α (Devereux et al. 1994) as well as emission from AGB stars in the bulge. As the flux from the nucleus fades towards longer wavelengths, the two spots above and below along the minor axis gain prominence. The prominence of the spot above the nucleus was noticed by Rice (1993) and confirmed by Haas et al. (1998). These spots appear to be the ends of a bar and the beginning of spiral arms. The location of these spots and appearance of the nuclear region (especially at $70 \mu\text{m}$) is similar to the triaxial bulge simulations of Berman (2001).

To investigate the morphology in more detail, the images have been deprojected assuming an inclination of 75° , and displayed in Fig. 3. Usually the inclination is picked visually to make the galaxy most spiral-like or circular in the deprojected frame. To be more objective, the inclination we use is the median value of the independently calculated inclinations of the spiral arm segments investigated by Braun (1991).

Arc-like structures dominate the morphology of the region inside the ~ 10 kpc ring and appear to be spiral arms with starting points at ends of a bar. The existence of a bar in M31 has been suggested in the past (Stark & Binney 1994). Since circularly symmetric objects will deproject into elongated bars, the evidence for a bar is based on the prominence of the two spots near the nucleus at $160 \mu\text{m}$, not on the appearance of a bar in the nuclear region at $24 \mu\text{m}$.

To determine the parameters of any spiral arms, Fig. 4 gives plots in polar and Cartesian coordinates of the locations of compact IR objects seen in all three MIPS bands. These regions are likely to be star forming regions (e.g., HII regions and OB associations) which are excellent spiral arm tracers. Point source photometry was done using

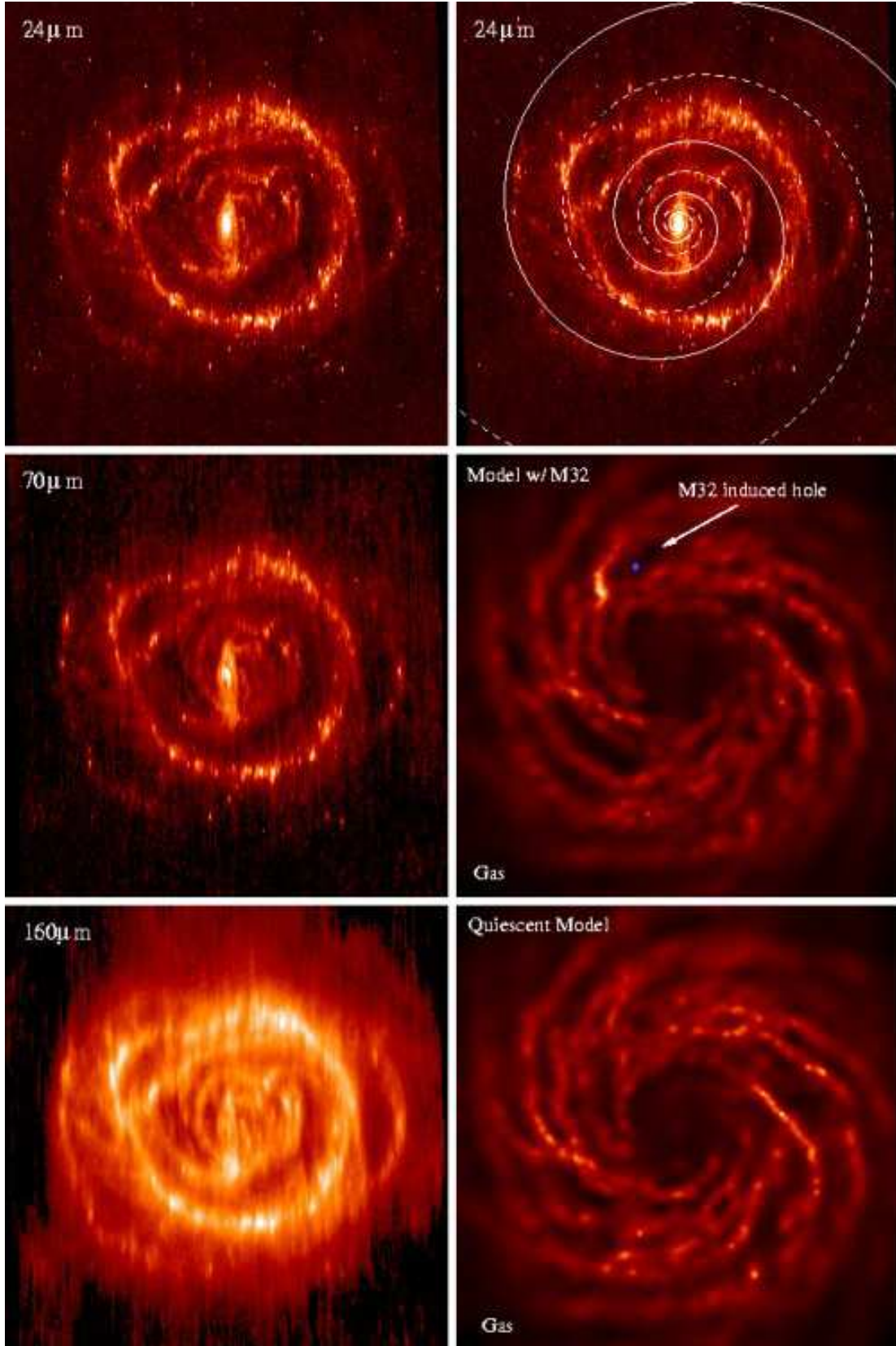


FIG. 3.— The MIPS images deprojected using an inclination of 75° are shown in the left column. The right column shows the 24 μm image with the spiral arms shown in Fig. 4 overplotted, the M31-M32 interaction model (M32 as a blue dot), and M31 quiescent model (see §4). The M31-M32 interaction model image gives the true location of M32. If deprojected with the same assumptions as the images, the location of M32 would shift off the image (within the $\sim 10'$ model insensitivity to the true position of M32). The model images give the integrated gas density which is nominally proportional to the dust given a constant gas-to-dust ratio (except in the inner region where it is clear that the gas-to-dust ratio likely varies significantly). The orientation of the images is the same as in Fig. 1 and the size is $3^\circ \times 3^\circ$.

StarFinder (Diolaiti et al. 2000) after convolving the 24 and 70 μm images to the 160 μm resolution using custom convolution kernels (Gordon et al., in prep.) ensuring the same physical regions were measured in the three MIPS bands.

In polar coordinates, a logarithmic spiral is a line with a non-zero slope and a circle is a horizontal line. The strongest feature is the wavy line around $\ln(\text{radius}) = 3.75$ representing the ~ 10 kpc ring. This wavy line is fit well by a circle offset from the nucleus by ($5.5'$, $3.0'$) with a radius of $43'/9.8$ kpc, except for the region around 200° where the ring splits. The remarkable circularity of this ring makes it difficult to explain this structure as spiral arm segments. Two logarithmic spirals are plotted which roughly follow the spiral structure. These trailing spirals have pitch angles of 9° and 9.5° , and are phase shifted by 166° . These two spirals trace most of the structure inside the ring as well as some of the structure outside the ring. These two spirals are not unique solutions, but reasonable given the disturbed nature of M31. The pitch angles used here are larger than found in previous work, consistent with not including the offset ~ 10 kpc ring as part of the spiral structure. We found that our simple logarithmic spirals plus an offset circle give as good or better representation of the MIPS sources than the Braun (1991) spiral arm segments when the segments were deprojected in the same manner as the MIPS sources.

Finding that M31 has an offset, star forming ring which is not just a superposition of spiral arm segments raises the question: “What is the origin of the ring?” The ring could be due to internal resonances which can cause three different types of rings: nuclear, inner, and outer (Buta 1986). The M31 ring is clearly not nuclear or an inner ring which is directly associated with bar. The M31 ring could be an outer ring which is associated with the outer Lindblad resonance/radius of corotation. The radius of corotation is placed around 18 kpc by Braun (1991). The ring could also be caused by interactions like those seen in the Cartwheel galaxy (Hernquist & Weil 1993). An interesting clue to the possible origin of the ring is the splitting of the ring by M32’s passage through M31’s disk (§4). Is this a coincidence or cause of the ring? A detailed study of the origin of M31’s ring is clearly needed.

While the logarithmic spirals plotted in Fig. 4 represent the data well, there are clear deviations from these spirals in addition to the well defined circle of star formation. The known interactions between M31 and its satellite galaxies M32 and NGC 205 imply these interactions may be the cause of the deviations from regular spiral structures.

4. DYNAMICAL MODELS

The dynamical effects that M32 and NGC 205 have on M31 were investigated by running a number of numerical simulations of the M31-M32 and M31-NGC 205 interactions using GADGET2 (Springel et al. 2001; Springel 2005). These simulations self-consistently model gravity and hydrodynamics. In addition, we have implemented star formation following Katz et al. (1996), cooling using the MAPPINGS III (<http://www.mso.anu.edu.au/~ralph/map.html>) collisional ionization equilibrium models for $[\text{Fe}/\text{H}] = -0.5$, and a combination of thermal and kinetic feedback from

supernovae (Navarro & White 1993, with $f_v = 0.1$) using the instantaneous recycling approximation. We used only the tree algorithm when calculating the gravitational forces as we found that the default TreePM method introduced unacceptably large numerical artifacts.

The initial conditions for M31 were the “M31a” equilibrium disk-bulge-halo model of Widrow & Dubinski (2005), with 132092, 48000, and 357192 particles in each component respectively. A randomly-sampled fraction of the resulting disk particles were turned into gas particles such that the radial gas density profile followed the sum of the HI (Braun et al., in prep.) and CO (Nieten et al. 2005) gas profiles except in the inner region where we assume a constant density to account for the mass of ionized gas. M32 and NGC 205 are modeled as point particles, with radial velocities taken from Mateo (1998). The current line-of-sight distances to the satellite galaxies were varied within the uncertainties of current estimates (M32: McConnachie et al. (2005); NGC 205: Ferrarese et al. (2000)), and the velocities in the plane of the sky were varied freely in order to find configurations where each satellite has recently passed through the disk of M31.

In Figure 3 we show an image of one such simulation of M31 after an interaction with M32, assuming that M32 currently lies 8 kpc behind the nucleus of M31, has a velocity in the plane of the sky of 200 km s^{-1} SSE, and has a mass of $1 \times 10^{10} M_\odot$ (3–5 times larger than current estimates (Mateo 1998)). We also show an image of a simulation with no satellite. The passage of M32 through the disk of M31 results in a burst of star formation that propagates outward through the disk resulting in a large hole similar in size and location to the observed splitting of the star forming ring. The location and age of the star forming region NGC 206 is consistent with this star formation (Hunter et al. 1996). We find that such a feature rapidly distorts due to differential rotation, and so its present symmetric appearance indicates that the disk passage occurred very recently (20 Myr ago in this model). If we use a mass of $2 \times 10^9 M_\odot$ for M32, as suggested by Mateo (1998), very little effect is seen on the disk of M31, suggesting that M32 may be more massive than previously thought. It is interesting to note that the input high density gas ring is pulled off-center ($\sim 1'$) by the satellite interaction, similar but smaller than the observed offset ($6.3'$). The simulated ring fragments into spiral arms and, therefore, is not as apparent as the observed ring.

The mass of NGC 205 is uncertain (Mateo (1998) calculates a mass of approximately $8 \times 10^8 M_\odot$) and therefore its ability to strongly affect the disk of M31 is equally uncertain. We have run a number of simulations of NGC 205, and while we can find orbits for which it passes through and temporarily distorts the spiral structure in the disk, we have been unable to find one which produces a hole that matches the observed split in the ring. However, an exhaustive search of the parameter space has not yet been carried out.

It is a generic feature in all of our models (with or without satellite interaction) that the gas in the central region of M31 ends up at a temperature greater than 10^4 K , consistent with the observation of ionized gas in the nuclear region. This behavior is not seen in models

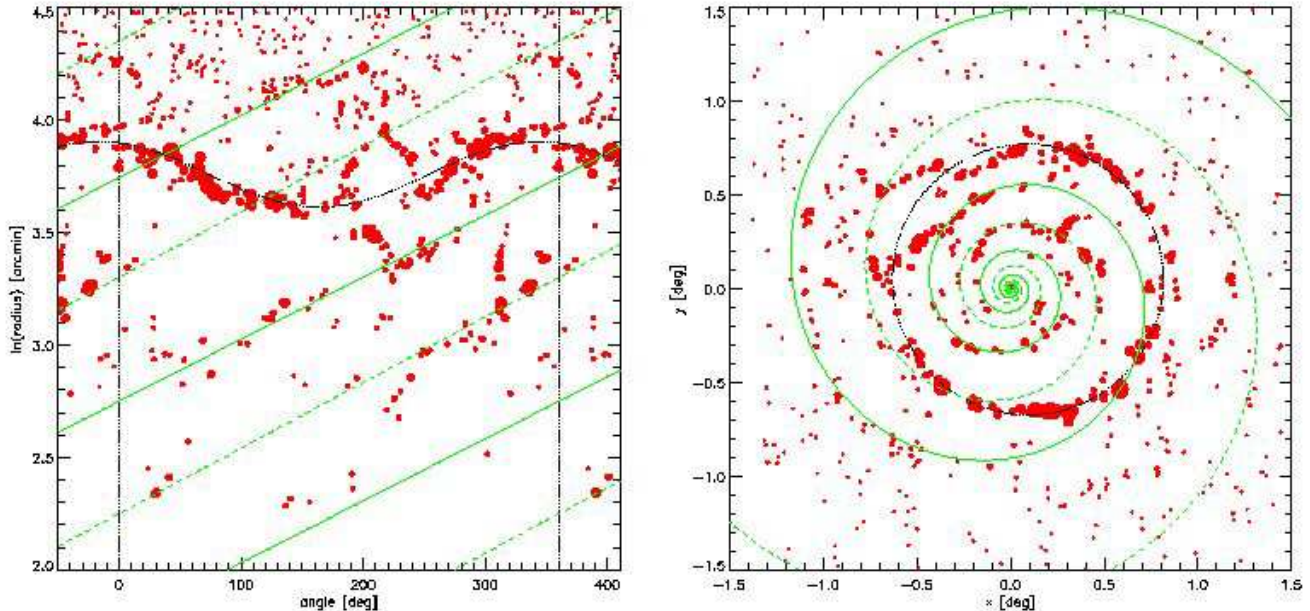


FIG. 4.— Polar and Cartesian plots showing the locations of point sources detected in all three MIPS bands at $160\ \mu\text{m}$ resolution. The symbols have been scaled by the measured $160\ \mu\text{m}$ fluxes. These plots are overlaid with two simple logarithmic spirals (green, one solid and one dashed) and an offset circle (black).

with a fully exponential gas disk; therefore, the hot nucleus is a direct result of the central depression of the gas density. As central depressions are commonly seen in the HI profiles of disk galaxies (e.g. Hewitt et al. 1983), our simulations suggest that a large fraction of the gas in the centers of disk galaxies is ionized.

5. CONCLUSIONS

We have presented new MIPS images of M31 at 24, 70, and $160\ \mu\text{m}$ which have higher spatial resolution and sensitivity than previous infrared images. These new images reveal the presence of two spiral arms in addition to a ring of star formation. The spiral arms appear to emanate from a bar in the nuclear region and can be roughly traced out beyond the ~ 10 kpc ring of star formation. The ring of star formation forms an almost complete circle which is offset from the nucleus and split near the location of M32. This ring of star formation and the disturbed spiral arms are indications that interactions may be affecting the morphology of M31. Dynamical models of M31 interacting with M32 predict morphology qualitatively similar to M31's (while models with NGC 205 instead of M32 give only small perturbations). Specifically, both the splitting and the offset of the star forming

ring are seen as well as copious spiral arms. It seems that M31 is not an undisturbed normal spiral galaxy, but one which has been significantly affected by interactions.

This paper presents a preview of the possibilities becoming available to understand M31. Data covering the majority of this galaxy are available in the X-ray (XMM, Trudolyubov et al., in prep.), ultraviolet (GALEX, Thilker et al. 2005), optical (Engelbracht et al., in prep.), mid-infrared (Spitzer/IRAC, Barmby et al., in prep.), infrared (this paper), HI (Braun et al., in prep.), CO (Nieten et al. 2005), and radio continuum (Beck et al. 1989); these will enable us to make detailed models on the impact that satellite galaxies have on the morphology of M31.

This work is based on observations made with the *Spitzer Space Telescope*, which is operated by the Jet Propulsion Laboratory, California Institute of Technology under NASA contract 1407. Support for this work was provided by NASA through Contract Number #1255094 issued by JPL/Caltech. JB thanks Paul Bourke for his visualization work and John Dubinski for providing an updated copy of the GalactICs code.

REFERENCES

- Arp, H. 1964, *ApJ*, 139, 1045
- Baade, W. & Arp, H. 1964, *ApJ*, 139, 1027
- Beck, R., et al. 1989, *A&A*, 222, 58
- Berman, S. 2001, *A&A*, 371, 476
- Braun, R. 1991, *ApJ*, 372, 54
- Brinks, E. & Shane, W. W. 1984, *A&AS*, 55, 179
- Buta, R. 1986, *ApJS*, 61, 609
- Byrd, G. G. 1978, *ApJ*, 226, 70
- . 1983, *ApJ*, 264, 464
- Devereux, N. A., et al. 1994, *AJ*, 108, 1667
- Diolaiti, E., et al. 2000, *A&AS*, 147, 335
- Ferguson, A. M. N., et al. 2002, *AJ*, 124, 1452
- Ferrarese, L., et al. 2000, *ApJS*, 128, 431
- Gordon, K. D., et al. 2005, *PASP*, 117, 503
- Guibert, J. 1974, *A&A*, 30, 353
- Haas, M., et al. 1998, *A&A*, 338, L33
- Habing, H. J., et al. 1984, *ApJ*, 278, L59
- Hernquist, L. & Weil, M. L. 1993, *MNRAS*, 261, 804
- Hewitt, J. N., Haynes, M. P., & Giovanelli, R. 1983, *AJ*, 88, 272
- Hodge, P. W. 1979, *AJ*, 84, 744
- . 1980, *AJ*, 85, 376
- Hubble, E. P. 1929, *ApJ*, 69, 103

- Hunter, D. A., et al. 1996, *ApJ*, 468, 633
Ibata, R., et al. 2005, *arXiv:astro-ph/0504164*
—. 2001, *Nature*, 412, 49
Katz, N., Weinberg, D. H., & Hernquist, L. 1996, *ApJS*, 105, 19
Kennicutt, R. C. 1998, *ARA&A*, 36, 189
Kraemer, K. E., et al. 2002, *AJ*, 124, 2990
Lewis, G. F., et al. 2004, *Publications of the Astronomical Society of Australia*, 21, 203
Loinard, L., et al. 1999, *A&A*, 351, 1087
Mateo, M. L. 1998, *ARA&A*, 36, 435
McConnachie, A. W., et al. 2005, *MNRAS*, 356, 979
Melchior, A.-L., et al. 2000, *MNRAS*, 312, L29
Navarro, J. F. & White, S. D. M. 1993, *MNRAS*, 265, 271
Nieten, C., et al. 2005, *A&A*
Odenwald, S., Newmark, J., & Smoot, G. 1998, *ApJ*, 500, 554
Rice, W. 1993, *AJ*, 105, 67
Rice, W., et al. 1988, *ApJS*, 68, 91
Rich, R. M., et al. 2005, *AJ*, 129, 2670
Rieke, G. H., et al. 2004, *ApJS*, 154, 25
Sato, N. R. & Sawa, T. 1986, *PASJ*, 38, 63
Simien, F., et al. 1978, *A&A*, 67, 73
Springel, V. 2005, *arXiv:astro-ph/0505010*
Springel, V., Yoshida, N., & White, S. D. M. 2001, *New Astronomy*, 6, 79
Stanek, K. Z. & Garnavich, P. M. 1998, *ApJ*, 503, L131
Stark, A. A. & Binney, J. 1994, *ApJ*, 426, L31
Thilker, D. A., et al. 2005, *ApJ*, 619, L67
van den Bergh, S. 1991, *PASP*, 103, 1053
Werner, M. W., et al. 2004, *ApJS*, 154, 1
Widrow, L. M. & Dubinski, J. 2005, *arXiv:astro-ph/0506177*